Melanoma and Lymphocyte Cell-Specific Targeting Incorporated into a Heat Shock Protein Cage Architecture

Michelle L. Flenniken,[1,2] Deborah A. Willits,[2,3]
Ann L. Harmsen,[4] Lars O. Liepold,[2,5]
Allen G. Harmsen,[4] Mark J. Young,[2,3,*]
and Trevor Douglas[2,5,*]
[1] Department of Microbiology
[2] Center for Bio-Inspired Nanomaterials
[3] Department of Plant Sciences
[4] Veterinary Molecular Biology Department
[5] Department of Chemistry and Biochemistry
Montana State University
Gaines Hall
Bozeman, Montana 59717

Summary

Protein cages, including viral capsids, ferritins, and heat shock proteins (Hsps), can serve as nanocontainers for biomedical applications. They are genetically and chemically malleable platforms, with potential as therapeutic and imaging agent delivery systems. Here, both genetic and chemical strategies were used to impart cell-specific targeting to the Hsp cage from *Methanococcus jannaschii*. A tumor vasculature targeting peptide was incorporated onto the exterior surface of the Hsp cage. This protein cage bound to $\alpha_v\beta_3$ integrin-expressing cells. Cellular tropism was also imparted by conjugating anti-CD4 antibodies to the exterior of Hsp cages. These Ab-Hsp cage conjugates specifically bound to CD4$^+$ cells. Protein cages have the potential to simultaneously incorporate multiple functionalities, including cell-specific targeting, imaging, and therapeutic agent delivery. We demonstrate the simultaneous incorporation of two functionalities, imaging and cell-specific targeting, onto the Hsp protein cage.

Introduction

The fusion of nanotechnology and medicine has the potential to transform diagnosis and therapeutics through the development of nanometer-scale (5–100 nm) therapeutic and imaging agent delivery systems with cell-specific tropisms. Incorporation of cell and tissue targeting allows for the potential of enhanced imaging capacity and precise therapeutic delivery. The objective of this work was to demonstrate that a single protein cage platform can simultaneously incorporate cell-specific targeting and imaging agent delivery.

Spherical protein cage architectures can be viewed as precisely assembled nanometer-scale containers. In nature, viral capsids, ferritins, and some heat shock proteins (Hsps) serve as examples of these architectures. In these examples, the protein cage architecture self-assembles from multiple copies of a limited number of protein subunits. The assembled subunits present three distinct surfaces for imparting function by design. These are the exterior of the cage, the interface between subunits, and regions exposed on the interior cavity. The subunits are highly amenable to both genetic and chemical modification, and these surfaces can be modified either individually or in combination without altering the assembly and overall architecture of the cage. Atomic resolution structural information identifies the precise location of amino acids within protein cage architectures. This detailed information enables the rational design of genetic mutants with novel functional properties. We and others have demonstrated that protein cages are robust platforms for chemical derivatization, genetic manipulation, metal chelation, and encapsulation [1–22]. Their multivalent nature allows for the incorporation of multiple functionalities within a single nanoparticle. We are exploring the potential medical applications of protein cage architectures.

Other nano-scale therapeutic delivery systems also being explored include: lipid micelles, silica nanoparticles, polysaccharide colloids, pegylated liposomes, polyamidoamine dendrimer clusters, and hydrogel dextran nanoparticles [9, 23–46]. Additionally, antibody-mediated therapeutic delivery has proven successful in both lab and clinical settings, and antibodies themselves may serve as therapeutic agents [47–64]. In this work, we demonstrate that protein cage platforms are an additional system to which medically relevant functionalities can be incorporated.

The field of cell-specific targeting has been significantly advanced by the in vivo use of phage display techniques to identify targeting peptides [24, 25, 29, 36, 37, 65–68]. Small peptides have been identified that target to the vasculature of a variety of tissues, organs, and tumors [69–72]. Targeting peptides linked to specific cargo molecules, such as therapeutic agents, proapoptotic peptides, and quantum dots were able to localize the cargo to the desired in vivo target [25, 29, 71, 73–76]. One characterized example is the targeting peptide RGD-4C (CDCRGDCFC), which binds $\alpha_v\beta_3$ and $\alpha_v\beta_5$ integrins that are prevalently expressed within tumor vasculature [18, 25, 62, 77, 78]. Work by Arap et al. demonstrated that RGD-4C-targeted doxorubicin enhanced tumor regression at therapeutic concentrations less than that required to demonstrate therapeutic efficacy with nontargeted doxorubicin [25]. Subsequently, many researchers have utilized the RGD-4C peptide motif for tumor targeting of liposomes, radiolabels, therapeutics, and adenoviral gene therapy vectors [62, 75, 76, 79–92]. The effects of RGD-4C targeted therapeutics are augmented due to the antiangiogenic property of RGD-4C itself [25, 62, 76, 80, 91, 92]. Due to the prior success of RGD-4C, it was chosen as a "proof of concept" targeting peptide for genetic incorporation into a small Hsp cage architecture.

In this study, we investigated the ability to introduce cell targeting capacity to protein cage architectures. Both peptides and antibodies were incorporated on the exterior surface of Hsp cages and tested for their ability to bind cell surface ligands. We also investigated

*Correspondence: myoung@montana.edu (M.J.Y.); tdouglas@chemistry.montana.edu (T.D.)

the ability to simultaneously encapsulate a cargo molecule on the Hsp cage interior along with targeting ligands on the exterior surface.

Results and Discussion

We have demonstrated that genetic addition of the RGD-4C peptide or chemical conjugation of an anti-CD4 monoclonal antibody (mAb) onto the exterior surface of the small Hsp cage architecture confers specific cell targeting capacity. In addition, we were able to load a cargo molecule, a fluorescent imaging agent (fluorescein), within the interior cavity of the Hsp cage. These results demonstrate the multifunctional capacity of protein cage architectures and their potential utility in medicine.

For these studies, we chose to use a small Hsp cage, which we previously established as a robust platform for genetic and chemical manipulation [4, 5]. The small Hsp cage from the hyperthermophilic archaeon, *Methanococcus jannaschii*, assembles from 24 identical subunits into a 12 nm diameter empty sphere [93]. In order to impart $\alpha_v\beta_3$ and $\alpha_v\beta_5$ integrin targeting capabilities to the Hsp cage, the RGD-4C peptide was genetically incorporated into a previously described Hsp variant (HspG41C) [4, 5]. Both of these integrins are prevalently expressed on angiogenic tumor vasculature [25, 62]. The HspG41C mutant presents unique reactive cysteine residues on the interior surface of the assembled cage for attachment of cargo molecules. Protein modeling, based on crystallographic data, indicates that C-terminal amino acid residues 140–146 are found on the exterior surface of the Hsp cage [93, 94]. An Hsp C-terminal RGD-4C fusion protein was genetically engineered to present exposed RGD-4C loops on the exterior of the protein cage. Glycine residues (SGG**CDCRGDCFC**G) were added both before and after the RGD-4C insert to extend the peptide away from the C terminus and allow for some structural flexibility. The insert was confirmed by DNA sequencing, and the new tumor-targeting Hsp cages were expressed and purified from an *Escherichia coli* expression system. Mass spectrometry verified the average subunit mass of HspG41C-RGD4C to be 17,814.3 compared to the predicted mass of 17,814.6 (see the Supplemental Data, available with this article online). The HspG41C-RGD4C mutant assembled as well as the wild-type protein cage (Figure 1). HspG41C-RGD4C protein cage purification did not require reducing agents to prevent intercage aggregation, suggesting that the four cysteines present in each RGD-4C loop are disulfide bonded.

Characterization of recombinant HspG41C-RGD4C protein cages by size exclusion chromatography, dynamic light scattering (DLS), and transmission electron microscopy (TEM) demonstrated that the overall spherical structure of the Hsp cage was not compromised due to the incorporation of the RGD-4C peptide (Figure 1). Size exclusion chromatography elution profiles of HspG41C-RGD4C cages indicate that the cages are slightly larger than the HspG41C parent cage lacking the targeting peptide (Figure 1) [5]. This observation was supported by DLS, which indicated a larger average diameter for the HspG41C-RGD4C cages (15.4 ± 0.3 nm [mean ± SD]) as compared to HspG41C (12.7 ± 0.5 nm)
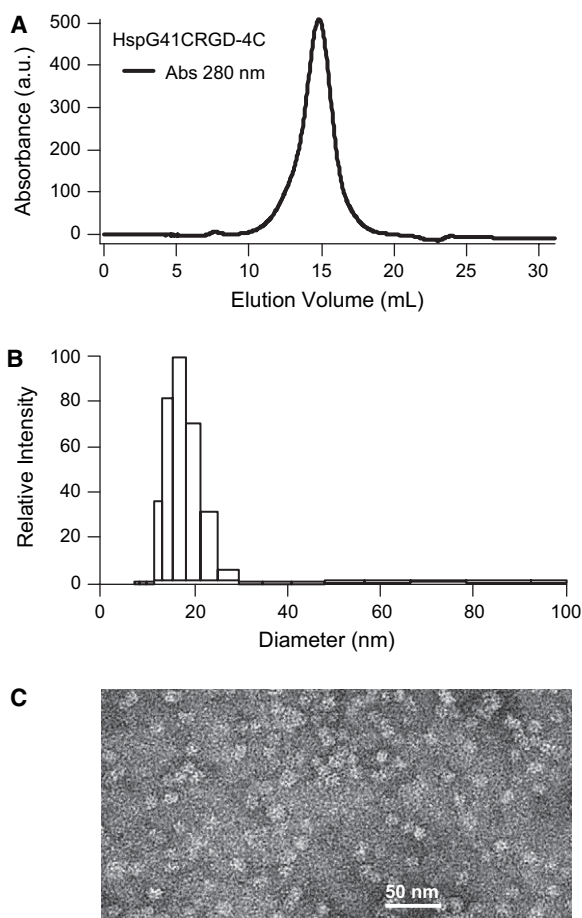
Figure 1. Characterization of the $\alpha_v\beta_3$ Integrin-Targeted HspG41C-RGD4C Protein Cage Architecture

(A) Size exclusion chromatography elution profile of HspG41C-RGD4C cages (Abs 280 nm).
(B) Dynamic light scattering analysis of HspG41C-RGD4C (average diameter 15.4 ± 0.3 nm).
(C) Transmission electron micrograph (TEM) of the HspG41C-RGD4C cages negatively stained with 2% uranyl acetate.

(Figure 1). TEM images of the HspG41C-RGD4C cages and HspG41C cages are indistinguishable (Figure 1) [5].

We chemically attached fluorescein molecules to cysteine residues on Hsp cages in order to study cell-specific targeting of HspG41C-RGD4C cages. This demonstrates that both cell targeting and imaging functionalities can be simultaneously incorporated into the Hsp protein cage architecture. The HspG41C-RGD4C has a total of 120 cysteines per cage (5 cysteines per subunit). Substoichiometric labeling with fluorescein-5-maleimide ensured that every cage displayed a significant fraction of unmodified cysteines within the RGD-4C sequence. The original RGD-4C peptides discovered by phage display were in a cyclic conformation due to intrapeptide disulfide bond formation [25, 29]. Likewise, we predicted that RGD-4C peptides presented on HspG41C-RGD4C architectures would also cyclize due to intrapeptide disulfide bond formation. Hsp-fluorescein-conjugated cages were purified from free fluorescein via size exclusion chromatography, and the covalent nature of the fluorescein-Hsp subunit linkage was demonstrated by
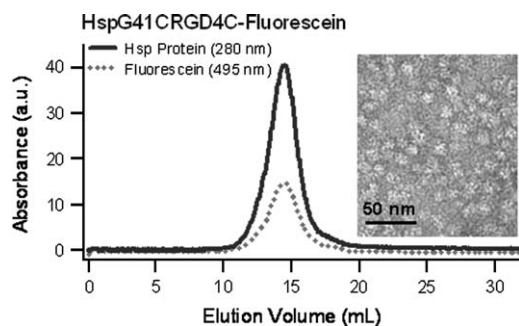
Figure 2. Characterization of Fluorescein-Labeled HspG41C-RGD4C Cages

Size exclusion chromatography elution profile of HspG41C-RGD4C cages. Coelution of the absorbance at 495 nm (fluorescein) and 280 nm (protein) illustrates that fluorescein is bound to intact Hsp cages. TEM micrograph (inset) also demonstrates the presence of intact Hsp cages.

SDS-polyacrylamide gel electrophoresis (SDS-PAGE) (Figure 2; Supplemental Data). Absorbance spectroscopy determined that, on average, there were 26 out of the 120 possible cysteines per cage labeled with fluoresceins; therefore, only a fraction of the cysteines within the RGD-4C were bound to fluorescein. Qualitative mass spectrometry analysis of fluorescein-labeled HspG41C-RGD4C subunits indicated that there are between one and five fluoresceins per subunit (Supplemental Data). Some of the RGD-4C peptides were presumably in "loop" conformation, whereas others were potentially linearized depending on the number of conjugated fluorescein-5-maleimides per subunit [5]. Data from mass spectrometry indicated the presence of both the disulfide and the free thiol form of the RGD-4C peptide. Previous structural studies of synthetic RGD-4C peptides in solution revealed that there are two predominant cyclic conformations, both of which bind $\alpha_v\beta_3$ integrin, although one (RGD-A) exhibited higher binding affinity [95]. However, in a second report, synthetically produced acyclic RGD-4C was shown to have higher binding affinity than the cyclic form [86]. Since the fluorescein-labeled HspG41C-RGD4C constructs most likely had a mixed presentation of "loop" and linearized RGD-4C targeting peptides, we hypothesized that they would bind $\alpha_v\beta_3$ integrin-expressing cells.

Epifluorescence microscopy was used to visualize fluorescently labeled HspG41C-RGD4C cages bound to $\alpha_v\beta_3$ integrin-expressing C32 melanoma cells in vitro [96, 97]. For all microscopy studies, C32 melanoma cells were grown on glass coverslips. Cell surface expression of $\alpha_v\beta_3$ integrin on C32 cells was verified by immunofluorescence utilizing a fluorescein-conjugated anti-$\alpha_v\beta_3$ mAb (LM609). HspG41C-RGD4C-fluorescein cages were observed to efficiently bind C32 cells as compared to control samples of Hsp cages without the RGD-4C peptide (Figure 3). For direct comparison of epifluorescence data, the concentration of fluorescein was normalized (2.5 μM), and the illumination intensity and the camera exposure were held constant. HspG41C-RGD4C-fluorescein protein cages were observed to efficiently bind to C32 melanoma cells as compared to controls of Hsp protein cages lacking the RGD-4C peptide (Figure 3). In order to ensure that HspG41C-RGD4C-fluorescein interaction with C32 cells was not mediated solely by exterior RGD-4C bound fluorescein, an additional mutant with surface-exposed cysteine residues (HspS121C) was also tested. The HspS121C-fluorescein cages bind fluorescein-5-maleimide via externally facing cysteines, but lack the RGD-4C targeting sequences. These control cages did not bind C32 cells at a level detectable by epifluorescence microscopy, indicating the cell binding observed for HspG41C-RGD4C was due to the presence of the RGD-4C peptide (Figure 3).

Fluorescence-activated cell sorting (FACS) was used to quantify the ability of fluorescein-labeled HspG41C-RGD4C cages to bind C32 melanoma cells. Adherent C32 melanoma cells were nonenzymatically disassociated from cell culture dishes and suspended in DPBS plus Ca^{2+}/Mg^{2+}. Fluorescently labeled Hsp cage preparations were incubated with cells on ice at a normalized fluorescein concentration of 2 μM and cells were washed prior to FACS. C32 melanoma cell-associated fluorescence was dramatically increased after incubation with HspG41C-RGD4C-fluorescein cages. The geometric mean (geo. mean) fluorescence intensity value of 1410 clearly indicated that targeted HspG41C-RGD4C cages exhibited cell binding in vitro (Figure 4A). C32 melanoma cells do exhibit a background level of autofluorescence with geo. mean fluorescence intensity value of 66 (Figure 4A). A positive control experiment, in which C32 melanoma cells were incubated with a fluorescein-conjugated anti-$\alpha_v\beta_3$ mAb, also showed the expected
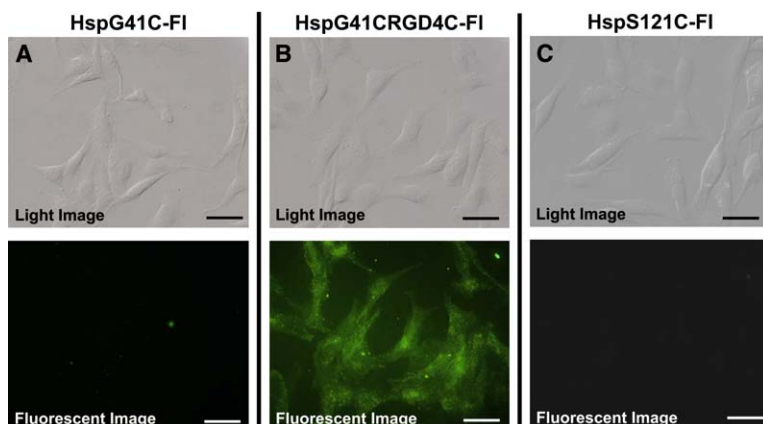

Figure 3. Epifluorescence Microscopy of C32 Melanoma Cells with Hsp Cage Fluorescein Conjugates

Cells were incubated with (A) nontargeted HspG41C-Fl cages with interiorly bound fluorescein, (B) $\alpha_v\beta_3$ integrin targeted HspG41CRGD4C-Fl cages and (C) nontargeted HspS121C-Fl cages with exteriorly bound fluorescein. C32 melanoma cells grown on coverslips were incubated with Hsp cage fluorescein conjugates and imaged by both light (top) and fluorescent microscopy (bottom). The fluorescein concentration for cage cell incubations was 2.5 μM, and all fluorescent images were taken at a standardized camera exposure time of 50 ms. Scale bar, 50 μm.
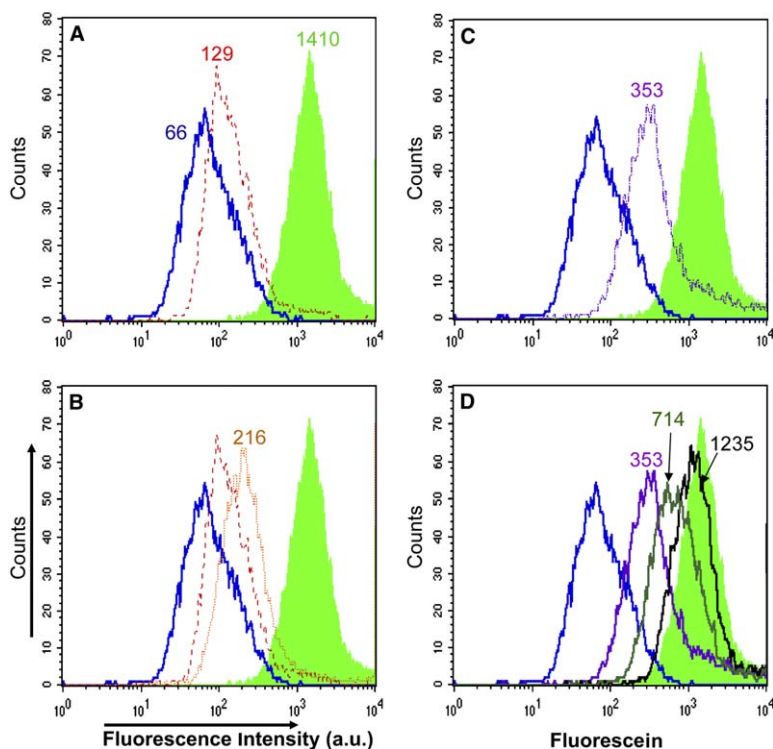
Figure 4. Specific Binding of HspG41CRGD4C-Fluorescein-Labeled Cages to C32 Melanoma Cells

The FACS data of C32 cells incubated with Hsp-fluorescein cages are plotted as histograms labeled with their corresponding geometric (geo.) mean fluorescence intensity values. The background level of C32 cell-associated fluorescence (blue solid line; geo. mean = 66) and the increased level of C32 cell-associated fluorescence due to binding of HspG41CRGD4C-Fl cages (green filled plot; geo. mean = 1410) are shown.

(A) Nontargeted cages HspG41C-fluorescein labeled interiorly (red dashed line; geo. mean = 129).

(B) Nontargeted HspS121C-Fl cages with exteriorly bound fluorescein (orange dotted line; geo. mean = 216).

(C) Anti-$\alpha_v\beta_3$ integrin mAb blocked C32 melanoma cells subsequently incubated with HspG41CRGD4C-Fl cages (dashed purple line; geo. mean = 353).

(D) mAb concentration-dependent blocking of $\alpha_v\beta_3$ integrin on C32 cells demonstrated by subsequent incubation of blocked cells with HspG41CRGD4C-Fl (2.4 μM subunit in the assembled cage, corresponding to 0.1 μM cage); 1.3 μM mAb (purple solid line; geo. mean = 353), cells blocked with 0.65 μM (green solid line; geo. mean = 714), 0.065 μM mAb (solid black line; geo. mean = 1235).

increase in fluorescence (geo. mean, 1037) associated with cell-specific binding of the antibody (Supplemental Data). FACS analysis of nontargeted cages (HspG41C-fluorescein inside; HspS121C-fluorescein outside) indicated low levels of nonspecific binding of protein cages and fluorescein to C32 melanoma cells (geo. mean intensities of 129 and 216, respectively, Figures 4A–4B). In all cases, these results were independent of incubation time, which ranged from 20 min to 2 hr (data not shown). The binding specificity of RGD-4C-targeted Hsp cages was tested with competition experiments. For these studies, C32 melanoma cells were preincubated with either unlabeled anti-$\alpha_v\beta_3$ mAb or unlabeled HspG41C-RGD4C prior to incubation with fluorescently labeled HspG41C-RGD4C cages. FACS analysis demonstrated a reduction of RGD-4C-targeted cage binding (Figures 4 and 5). As stated above, for FACS analysis, the fluorescein concentration was normalized (2 μM);
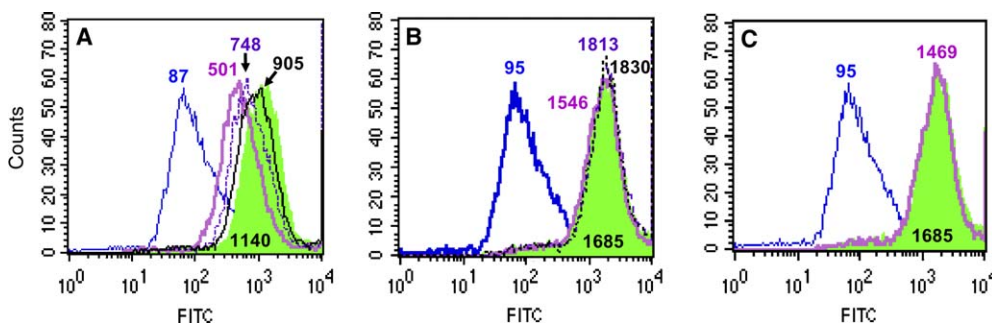

Figure 5. HspG41CRGD4C-Fluorescein Cage Interaction with C32 Melanoma Cells is Blocked by Unlabeled HspG41C-RGD4C but Not by HspG41C or Albumin

FACS data from C32 melanoma cells incubated with an unlabeled blocking protein (HspG41C-RGD4C, HspG41C, or bovine albumin) prior to incubation with HspG41CRGD4C-fluorescein cages are plotted as histograms labeled with their corresponding geo. mean fluorescence intensity values. The background level of C32 cell-associated fluorescence (blue solid line; geo. means = 87 and 95) and the increased level of C32 cell-associated fluorescence due to binding of HspG41CRGD4C-Fl cages (50 μg/ml) (green filled plots; geo. mean = 1140 and 1685), in the absence of any blocking protein, are shown.

(A) Unlabeled HspG41C-RGD4C concentration-dependent blocking; 5000 μg/ml (light purple solid line; geo. mean = 501), 500 μg/ml (dark purple dashed line; geo. mean = 748), cells blocked with 50 μg/ml (solid black line; geo. mean = 905).

(B) Unlabeled HspG41C does not block HspG41CRGD4C-Fl cage interaction with C32 cells; 5000 μg/ml (light purple solid line; geo. mean = 1546), 500 μg/ml (dark purple dotted line; geo. mean = 1813), cells blocked with 50 μg/ml (solid black line; geo. mean = 1830).

(C) Unlabeled bovine albumin (5000 μg/ml) does not block HspG41CRGD4C-Fl cage interaction with C32 cells (light purple solid line; geo. mean = 1469).

Note: All FACS machine settings were identical, but data set (A) was collected on a different day than sets (B) and (C).
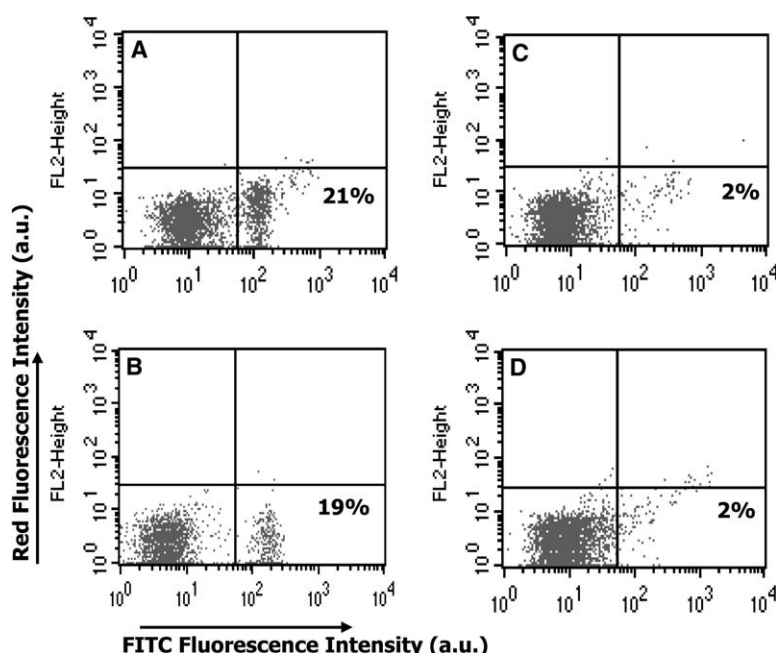
Figure 6. Specific Binding of Anti-CD4 mAb-Conjugated HspG41C-Fluorescein Cages to CD4$^+$ Lymphocytes

FACS analysis of murine splenocytes incubated with: (A) anti-CD4 mAb HspG41C fluorescein cage conjugates (Ab-Hsp-Fl) bound 21% of cells within this population; (B) anti-CD4 mAb-fluorescein demonstrated that 19% of this splenocyte population is CD4$^+$; (C) CD4$^+$ cells blocked with unlabeled anti-CD4 mAb, then subsequently exposed to Ab-Hsp-Fl cage conjugates, demonstrated a low level of nonspecific binding (2%); corresponding to (D) nontargeted HspG41C-fluorescein cages (2%).

this amount of fluorescein corresponds to 50 μg/ml (2.4 μM) HspG41C-RGD4C subunit in the assembled cage (corresponding to 0.1 μM cage); the ratio of fluorescein per subunit is near one to one. The degree of both antibody and HspG41C-RGD4C blocking was concentration-dependent. In order to compare the effectiveness of different blocking proteins, we compared them on a molar basis. At anti-$\alpha_v\beta_3$ integrin mAb concentrations of 0.065 μM (10 μg/ml), minimal inhibition was observed. At 0.65 μM (100 μg/ml) some inhibition was evident, and finally, at 1.3 μM (200 μg/ml), binding was inhibited to levels corresponding to that of nontargeted cages (Figure 4D). Likewise, unlabeled HspG41C-RGD4C reduces the binding of HspG41CRGD4C-Fl in a concentration-dependent manner (Figure 5). Blocking of the RGD-4C-$\alpha_v\beta_3$ integrin interaction was demonstrated to be specific, since equivalent amounts of either HspG41C or bovine albumin (fraction V) did not decrease the binding of HspG41CRGD4C-Fl to C32 melanoma cells (Figure 5). Together, these data illustrate the effective genetic introduction of $\alpha_v\beta_3$ integrin targeting capacity to the Hsp cage architecture.

The versatility of protein architectures for cell-specific targeting was demonstrated by the chemical introduction of lymphocyte targeting to Hsp architectures. An anti-CD4 mAb (GK1.5; American Type Culture Collection [ATCC], Manassas, VA) was conjugated to fluorescein-labeled HspG41C cages via the heterobifunctional crosslinker sulfo-SMCC (sulfosuccinimidyl 4-[N-maleimidomethyl] cyclohexane-1-carboxylate). Size exclusion chromatography was utilized to purify anti-CD4-HspG41C-fluorescein cage conjugates (Ab-Hsp-Fl) from HspG41C-fluorescein cages. The elution profile indicated that the Ab-Hsp-Fl cage conjugates were larger than HspG41C-Fl cages, and DLS confirmed the size increase from 12.2 nm to 22 ± 0.1 nm diameter (Supplemental Data).

FACS and epifluorescence microscopy were used to investigate binding of anti-CD4-HspG41C-fluorescein

(Ab-Hsp-Fl) cages to CD4$^+$ cells within a murine splenocyte population. A comparison of epifluorescence microscope images in which Ab-Hsp-Fl, Hsp-Fl, or Ab-Fl were each combined individually with murine splenocytes illustrated that Ab-Hsp-Fl bound to a similar number of cells as the Ab-Fl-positive control (Supplemental Data). FACS was used for quantitative analysis of this interaction. Ab-Hsp-Fl cages specifically bound to 21% of the total cells within this population (Figure 6A). This level of binding is consistent with the percentage of CD4$^+$ cells within this murine splenocyte population as determined by binding of a fluorescein conjugated anti-CD4 mAb to 19% of this murine splenocyte population (Figure 6B). Further confirmation of binding specificity was obtained from antibody blocking experiments. Splenocytes were incubated with unlabeled anti-CD4 mAb, washed to remove unbound blocking antibody, and subsequently incubated with Ab-Hsp-Fl cage conjugates. FACS analysis of this blocking experiment demonstrated that only 2% of the population exhibited cell-associated fluorescence (Figure 6C). This percentage of cell fluorescence corresponds to that observed with nontargeted HspG41C-fluorescein cages (2%) (Figure 6D). The observed binding of Ab-Hsp-Fl cages to 21% of the murine splenocyte population encompasses both the specific binding to CD4$^+$ lymphocytes (19%) on top of a small, nonspecific level of background association (2%). This indicates that immuno-targeted protein cages effectively target to specific cells within a mixed population.

In this work, the 12 nm diameter Hsp cage was both genetically and chemically modified to incorporate cell-specific targeting properties. Genetic incorporation of $\alpha_v\beta_3$ integrin binding RGD-4C peptide onto the exterior surface of Hsp cages conferred cell-specific targeting capabilities to this protein cage architecture. It is expected that many other cell targeting peptides, especially those discovered by in vivo phage display library techniques, could also be incorporated into this and

other protein cage architectures. Chemical linkage of an anti-CD4-antibody to Hsp cages, and subsequent targeting of a subset of CD4+ cells within a population of murine splenocytes, demonstrated the success and possibilities of immuno-targeted Hsp cages. Fluorescein, an imaging agent, was covalently linked to protein cages, demonstrating that these architectures can simultaneously incorporate multiple functionalities, including cell-specific targeting and imaging agent delivery.

Significance

The overall significance of this research is that it advances the utility of protein cage nanocontainers as platforms for combined cell-specific-targeted and imaging agent-targeted delivery systems. This opens exciting avenues for the incorporation and cell-specific delivery of other cargo molecules, such as magnetic resonance (MR) imaging and therapeutic agents. We demonstrate that the Hsp cage architecture can be genetically and chemically modified to impart mammalian cell targeting capacity. This work also demonstrates the ability to simultaneously incorporate cell targeting and imaging agents within a single protein cage. Protein cage architectures are precisely defined monodisperse molecular platforms with inherent genetic and chemical versatility. A library of protein cage architectures is available, ranging in size from 9 to > 100 nm diameter, extending the utility of this approach to diverse applications.

Experimental Procedures

Genetic Engineering of $\alpha_v\beta_3$ Integrin Targeting HspG41C-RGD4C

Methanococcus jannaschii genomic DNA was obtained from ATCC (43607). As described previously, the gene encoding the small Hsp (Mj HSP16.5) was polymerase chain reaction (PCR)-amplified and cloned into NdeI/BamHI restriction sites of the PET-30a(+) vector (Novagen, Madison, WI) for expression of the full-length protein with no additional amino acids. PCR-mediated site-directed mutagenesis was employed to replace the glycine at position 41 with a unique cysteine residue, therefore generating the HspG41C mutant [5]. Deletion of the HSP-stop codon directly upstream of the BamHI site was also accomplished by PCR-mediated site-directed mutagenesis. This deletion allowed for the insertion of additional sequence into the BamHI site to create the RGD-4C (CDCRGDCFC) carboxyl-terminal fusion protein engineered to present exposed RGD-4C loops on the exterior of the protein cage. The HspG41C-RGD4C fusion protein was engineered to have extra glycine residues (italicized below), both before and after the RGD-4C insert, to extend the insert away from the C terminus and allow some structural flexibility. Complimentary RGD-4C encoding primers with gatc overhangs for cloning into the BamHI site (+sense primer: 5′ ga tct gga gga tgc gac tgc cgc gga gac tgc ttc tgc gga taa gga 3′; encoding S *G G* C D C R G D C F C *G* stop) were mixed at a 1:1 molar ratio, annealed, and treated with kinase (Promega, Madison, WI). These inserts were subsequently ligated into an alkaline phosphatased, BamHI digested vector overnight at 17°C and transformed into XL-2 ultracompetant E. coli (Stratagene, La Jolla, CA). Transformants were screened for the presence of the RGD-4C insert and confirmed by sequencing the PCR amplified product on an ABI 310 automated capillary sequencer with BigDye Chain termination sequence technology (Applied Biosystems, Foster City, CA).

HspG41C-RGD4C Cage Purification and Characterization
All small Hsp cages (HspG41C, HspS121C, and HspG41C-RGD4C) were purified from an E. coli heterologous expression system as previously described [5]. One liter cultures of E. coli (BL21 [DE3] B

strain) containing pET-30a(+) MjHsp16.5 plasmid were grown overnight in LB plus kanamycin medium (37°C, 220 rpm). Cells were harvested by centrifugation at 3700 × g for 15 min (Heraeus 3334 rotor, Sorvall Centrifuge) and resuspended in 30 ml of 100 mM HEPES, 50 mM NaCl, pH 8.0. Lysozyme, DNase, and RNase were added to final concentrations of 50, 60, and 100 µg/ml, respectively. The sample was incubated for 30 min at room temperature, French pressed (American Laboratory Press Co., Silver Springs, MD), and sonicated on ice (Branson Sonifier 250, power 4, duty cycle 50%, 3 × 5 min with 3 min intervals). Bacterial cell debris was removed via centrifugation for 20 min at 12,000 × g. The supernatant was heated for 15 min at 65°C, thereby denaturing many E. coli proteins. The supernatant was centrifuged for 20 min at 12,000 × g and purified by gel filtration chromatography (Superose-6, Amersham-Pharmacia, Piscataway, NJ; Bio-Rad Duoflow, Hercules, CA). Recombinant HspG41C-RGD4C protein cages were routinely characterized by size exclusion chromatography (Superose 6, Amersham Pharmacia), DLS (Brookhaven 90Plus, Brookhaven, NY), TEM (Leo 912 AB), SDS-PAGE, and mass spectrometry (Acquity/Q-Tof micro; Waters, Milford, MA). Protein concentration was determined by absorbance at 280 nm divided by the published extinction coefficient (9322 M^{-1} cm^{-1}) [93].

Labeling Hsp with Activated Fluorescein Dye
Cysteine containing Hsp cages (100 mM HEPES, 50 mM NaCl, pH 6.5) were reacted with fluorescein-5-maleimide (Molecular Probes, Eugene, OR) in concentrations ranging from 1–6 molar equivalents per Hsp subunit for 30 min at room temperature, followed by overnight incubation at 4°C. Fluorescein-labeled Hsp cages were purified from free dye by size exclusion chromatography (DPBS pH 7.4). The number of fluorescein molecules per cage was calculated from absorbance spectra [4, 5]. For example, HspG41C-RGD4C (2 mg/ml; 112 µM subunit) reacted with 2.2 molar equivalents of fluorescein-5-maleimide (246 µM) per Hsp subunit resulted in HspG41C-RGD4C cages with an average of 26.2 fluoresceins per cage (or 1.09 fluoresceins per subunit). The number of fluoresceins per cage was quantified by absorbance spectroscopy [5].

C32 Amelanotic Melanoma Cell Culture
Human amelanotic melanoma cell line, C32, was obtained from ATCC (CRL-1585). C32 cells were propagated in Minimum Essential Medium Eagle (MEME) (ATCC 30–2003) supplemented with 10% fetal bovine serum (Atlanta Biologicals, Norcross, GA), penicillin (100 U/ml), and streptomycin (100 µg/ml) (Sigma, St. Louis, MO) at 37°C, in a 5% CO$_2$ incubator.

Mass Spectrometry
Hsp samples were analyzed by liquid chromatography/electrospray mass spectrometry (LC/MS) (Acquity/Q-Tof micro; Waters). HspG41C-RGD4C and derivatized HspG41C-RGD4C (5–15 µl, 0.3–0.5 mg/ml) were injected onto a C8 column (208TP5115, Vydac) and eluted with an H$_2$O–acetonitrile linear gradient (eluent A: 0.1% formic acid in water; eluent B: 0.05% trifluoroacetic acid in acetonitrile).

Epifluorescence Microscopy of C32 Melanoma Cells
Epifluorescence microscopy was performed on an Axioscope 2-Plus microscope (Zeiss) utilizing version 4.1 software and an Axiocam high-resolution camera (Hrc). For all microscopy studies, C32 melanoma cells were grown on glass coverslips to ~60% confluency (MEME + 10% FBS), in the presence of penicillin (100 units/ml) and streptomycin (100 µg/ml) (Sigma). C32 expression of the RGD-4C target receptor, $\alpha_v\beta_3$ integrin, was verified by immunofluorescence utilizing a fluorescein-conjugated anti-$\alpha_v\beta_3$ mAb (LM609) (MAB1976F; Chemicon, Temecula, CA).

C32 cells grown on coverslips were incubated with Hsp cages in serum-free medium for 30 min at 37°C in a 5% CO$_2$ incubator. The fluorescein concentration of the Hsp-fluorescein preparations was normalized to 2.5 µM to facilitate comparison. After incubation, the cells were washed five times with Dulbecco's phosphate-buffered saline (DPBS; Sigma), fixed with 4% paraformaldehyde for 10 min, washed with DPBS, and then mounted on slides in Vectashield mounting medium (Burlingame, CA). Illumination intensity and camera exposure times were held constant.

FACS Analysis of C32 Cells Incubated with Fluorescein-Conjugated Hsp Cages

Flow cytometry was performed on a FACSCalibur (Becton Dickinson, Mountain View, CA) and analyzed with Cell Quest software (Becton Dickinson). Adherent C32 melanoma cells were nonenzymatically disassociated from cell culture dishes with DPBS without Ca^{2+} or Mg^{2+} plus 1% ethylenediaminetetraacetic acid (EDTA; ∼25 mM) (for about 2 min at room temperature), washed once with serum-containing medium, and finally suspended in DPBS plus Ca^{2+}/Mg^{2+} at 2.1×10^6 cells/ml. Experiments were carried out both in the presence and absence of 1% FBS in the buffer; results were similar in both conditions. Fluorescently labeled cage preparations (normalized to 2 μM fluorescein) were incubated with cells on ice from 20 min to 2 hr. After incubation, the cells were washed five times with DPBS (both with and without Ca^{2+}/Mg^{2+}), and suspended in DPBS plus 1% FBS for FACS analysis; 10,000 events were counted for each condition. Both the anti-$\alpha_v\beta_3$ mAb (LM609) (Chemicon MAB1976Z) and the corresponding fluorescein-conjugated anti-$\alpha_v\beta_3$ mAb (Chemicon MAB1976F) were used for FACS analysis.

HspG41C-Fluorescein Anti-CD4 Antibody Conjugation

Fluorescein-labeled HspG41C protein cages were conjugated to anti-CD4 monoclonal antibodies (generated from ATCC GK1.5) via a heterobifunctional cross-linker, sulfosuccinimidyl 4-(N-maleimidomethyl) cyclohexane-1-carboxylate (sulfo-SMCC; Pierce, Rockford, IL). First, the antibodies (6.5 mg/ml in PBS, [pH 7.4]) were partially reduced with 10 mM tris(2-carboxyethyl)phosphine (TCEP) in the presence of 10 mM EDTA, with the final pH adjusted to 6.5, and incubated for 2 hr at room temperature [98]. Simultaneously, the exposed lysines (amines) of HspG41C-fluorescein cages (0.25 mg/ml; 15 μM subunit in 500 μl DPBS, [pH 7.4]; 11 fluoresceins per cage) were reacted with the sulfo-NHS-ester component of the sulfo-SMCC linker (added in excess 0.5 mg). The Hsp cage plus linker reaction was incubated at room temperature for 1 hr, followed by the removal of free sulfo-SMCC linker by size exclusion chromatography (desalting column; Pierce). The reduced anti-CD4 antibodies were combined with the HspG41C-fluorescein-SMCC cages and incubated for 3 hr before final purification of anti-CD4-HspG41C-fluorescein cage (Ab-Hsp) conjugates by size exclusion chromatography (Superose 6, Amersham-Pharmacia).

Murine Splenocyte Preparation

A BALB/c mouse spleen was homogenized in Hank's balanced salt solution (Mediatech, Herndon, VA) by pushing it through a 60 gauge stainless-steel mesh; the homogenate was filtered through 100 μm nylon mesh and centrifuged at $200 \times g$ for 10 min. The supernatant was discarded and the cell pellet suspended in 5 ml ACK lysis buffer (150 mM NH_4Cl, 1 mM $KHCO_3$, 0.1 mM Na_2EDTA) for 5 min at room temperature to lyse unwanted red blood cells. Lysis was stopped via the addition of PBS plus 2% donor calf serum (25 ml). The remaining white blood cells were pelleted by centrifugation at $200 \times g$ for 10 min and suspended in PBS plus 2% donor calf serum (2×10^7 cells/ml) containing anti-mouse Fc receptor antibody (from HB-197, ATCC) in order to prevent nonspecific binding of antibodies to the Fc receptor on lymphocytes. Cells were incubated on ice until binding assays were performed.

Epifluorescence Microscopy of Splenocytes

Aliquots of murine splenocytes were combined with equal volumes of each of the following: (A) anti-CD4-HspG41C-fluorescein (Ab-Hsp-Fl) cages, (B) fluorescein-conjugated anti-CD4 mAb (positive control), and (C) HspG41C-fluorescein cages (nontargeted control), and incubated for 30 min on ice. Following incubation, the cells were washed three times with PBS containing 2% donor calf serum. The cells were wet-mounted prior to epifluorescence microscopy with a Nikon Eclipse E800 microscope, equipped with a Nikon DMX1200 digital camera utilizing MetaVue software. Illumination intensity and camera exposure times were held constant.

FACS Analysis of Splenocytes Incubated with Anti-CD4 mAb-Conjugated Hsp Cages

FACS was performed on a FACSCalibur and analyzed with Cell Quest software. Aliquots of murine splenocytes were combined with equal volumes of each of the following: (A) anti-CD4-HspG41C-fluorescein (Ab-Hsp-Fl) cages, (B) fluorescein conjugated anti-CD4 mAb (positive control), and (C) HspG41C-fluorescein cages (nontargeted control), and incubated for 30 min on ice. Following incubation, the cells were washed in PBS containing 2% donor calf serum in preparation for FACS. FACS analysis was performed on a gated murine splenocyte cell population. For anti-CD4 mAb blocking experiments, splenocytes were incubated for 30 min with unlabeled anti-CD4 mAb and washed to remove unbound blocking antibody prior to incubation with Ab-Hsp-Fl cage conjugates.

Supplemental Data

Supplemental Data, including Figures S1–S6, are available at http://www.chembiol.com/cgi/content/full/13/2/161/DC1/.

References

1. Bulte, J.W.M., Douglas, T., Mann, S., Frankel, R.B., Moskowitz, B.M., Brooks, R.A., Baumgarner, C.D., Vymazal, J., and Frank, J.A. (1993). Magnetoferritin: biomineralization as a novel approach in the design of iron oxide-based MR contrast agents. Inv. Rad. 29 (Suppl. 2), S214–S216.

2. Bulte, J.W.M., Douglas, T., Mann, S., Frankel, R.B., Moskowitz, B.M., Brooks, R.A., Baumgarner, C.D., Vymazal, J., Strub, M.-P., and Frank, J.A. (1994). Magnetoferritin: characterization of a novel superparamagnetic MR contrast agent. J. Magn. Reson. Imaging. 4, 497–505.

3. Douglas, T., and Young, M. (1998). Host-guest encapsulation of materials by assembled virus protein cages. Nature 393, 152–155.

4. Flenniken, M.L., Liepold, L.O., Crowley, B.E., Willits, D.A., Young, M.J., and Douglas, T. (2005). Selective attachment and release of a chemotherapeutic agent from the interior of a protein cage architecture. Chem. Commun. (Camb.) 447–449.

5. Flenniken, M.L., Willits, D.A., Brumfield, S., Young, M.J., and Douglas, T. (2003). The small heat shock protein cage from Methanococcus jannaschii is a versatile nanoscale platform for genetic and chemical modification. Nano Lett. 3, 1573–1576.

6. Chatterji, A., Burns, L.L., Taylor, S.S., Lomonossoff, G.P., Johnson, J.E., Lin, T., and Porta, C. (2002). Cowpea mosaic virus: from the presentation of antigenic peptides to the display of active biomaterials. Intervirology 45, 362–370.

7. Allen, M., Willits, D., Mosolf, J., Young, M., and Douglas, T. (2002). Protein cage constrained synthesis of ferrimagnetic iron oxide nanoparticles. Adv. Mater. 14, 1562–1565.

8. Allen, M., Willits, D., Young, M., and Douglas, T. (2003). Constrained synthesis of cobalt oxide nano-materials in the 12-subunit protein cage from Listeria innocua. Inorg. Chem. 42, 6300–6305.

9. Allen, T.M., and Cullis, P.R. (2004). Drug delivery systems: entering the mainstream. Science 303, 1818–1822.

10. Douglas, T. (1996). Biomimetic synthesis of nanoscale particles in organized protein cages. In Biomimetic Approaches in Materials Science, S. Mann, ed. (New York: VCH Publishers), pp. 91–115.

11. Douglas, T., Allen, M., and Young, M. (2002). Self-assembling protein cage systems and applications in nanotechnology. In Polyamides and Complex Proteinaceous Materials I, Volume 7, S.R. Fahnestock and A. Steinbuchel, eds. (Weinheim, Germany: Wiley-VCH), p. 517.

12. Douglas, T., Strable, E., Willits, D., Aitouchen, A., Libera, M., and Young, M. (2002). Protein engineering of a viral cage for constrained nano-materials synthesis. Adv. Mater. *14*, 415–418.

13. Douglas, T., and Young, M. (1999). Virus particles as templates for materials synthesis. Adv. Mater. *11*, 679–681.

14. Hooker, J.M., Kovacs, E.W., and Francis, M.B. (2004). Interior surface modification of bacteriophage MS2. J. Am. Chem. Soc. *126*, 3718–3719.

15. Gillitzer, E., Willits, D., Young, M., and Douglas, T. (2002). Chemical modification of a viral cage for multivalent presentation. Chem. Commun. (Camb.) 2390–2391.

16. Klem, M.T., Willits, D., Solis, D.J., Belcher, A.M., Young, M., and Douglas, T. (2005). Bio-inspired synthesis of protein encapsulated copt nanoparticles. Adv. Func. Mater. *15*, 1489–1494.

17. Mao, C., Solis, D.J., Reiss, B.D., Kottmann, S.T., Sweeney, R.Y., Hayhurst, A., Georgiou, G., Iverson, B., and Belcher, A.M. (2004). Virus-based toolkit for the directed synthesis of magnetic and semiconducting nanowires. Science *303*, 213–217.

18. Koivunen, E., Wang, B., and Ruoslahti, E. (1995). Phage libraries displaying cyclic peptides with different ring sizes: ligand specificities of the RGD-directed integrins. Biotechnology (N. Y.) *13*, 265–270.

19. Wang, Q., Kaltgrad, E., Lin, T.W., Johnson, J.E., and Finn, M.G. (2002). Natural supramolecular building blocks: wild-type cowpea mosaic virus. Chem. Biol. *9*, 805–811.

20. Wang, Q., Lin, T.W., Johnson, J.E., and Finn, M.G. (2002). Natural supramolecular building blocks: cysteine-added mutants of cowpea mosaic virus. Chem. Biol. *9*, 813–819.

21. Wang, Q., Lin, T.W., Tang, L., Johnson, J.E., and Finn, M.G. (2002). Icosahedral virus particles as addressable nanoscale building blocks. Angew. Chem. Int. Ed. *41*, 459–462.

22. Allen, M.A., Leipold, L.O., Bulte, J.W.M., Basu, G., Zywicke, H.A., Frank, J.A., Young, M., and Douglas, T. (2005). Paramagnetic viral nanoparticles as potential high-relaxivity MRI contrast agents. Magn. Reson. Med. *54*, 807–812.

23. Roy, I., Ohulchanskyy, T.Y., Pudavar, H.E., Bergey, E.J., Oseroff, A.R., Morgan, J., Dougherty, T.J., and Prasad, P.N. (2003). Ceramic-based nanoparticles entrapping water-insoluble photosensitizing anticancer drugs: a novel drug-carrier system for photodynamic therapy. J. Am. Chem. Soc. *125*, 7860–7865.

24. Arap, W., Pasqualini, R., and Ruoslahti, E. (1998). Chemotherapy targeted to tumor vasculature. Curr. Opin. Oncol. *10*, 560–565.

25. Arap, W., Pasqualini, R., and Ruoslahti, E. (1998). Cancer treatment by targeted drug delivery to tumor vasculature in a mouse model. Science *279*, 377–380.

26. Braslawsky, G.R., Edson, M.A., Pearce, W., Kaneko, T., and Greenfield, R.S. (1990). Antitumor activity of adriamycin (hydrazone-linked) immunoconjugates compared with free adriamycin and specificity of tumor cell killing. Cancer Res. *50*, 6608–6614.

27. Braslawsky, G.R., Kadow, K., Knipe, J., McGoff, K., Edson, M., Kaneko, T., and Greenfield, R.S. (1991). Adriamycin(hydrazone)-antibody conjugates require internalization and intracellular acid hydrolysis for antitumor activity. Cancer Immunol. Immunother. *33*, 367–374.

28. Brigger, I., Dubernet, C., and Couvreur, P. (2002). Nanoparticles in cancer therapy and diagnosis. Adv. Drug Deliv. Rev. *54*, 631–651.

29. Ellerby, H.M., Arap, W., Ellerby, L.M., Kain, R., Andrusiak, R., Rio, G.D., Krajewski, S., Lombardo, C.R., Rao, R., Ruoslahti, E., et al. (1999). Anti-cancer activity of targeted pro-apoptotic peptides. Nat. Med. *5*, 1032–1038.

30. Emerich, D.F., and Thanos, C.G. (2003). Nanotechnology and medicine. Expert Opin. Biol. Ther. *3*, 655–663.

31. Fundaro, A., Cavalli, R., Bargoni, A., Vighetto, D., Zara, G.P., and Gasco, M.R. (2000). Non-stealth and stealth solid lipid nanoparticles (SLN) carrying doxorubicin: pharmacokinetics and tissue distribution after i.v. administration to rats. Pharmacol. Res. *42*, 337–343.

32. Hallahan, D., Geng, L., Qu, S., Scarfone, C., Giorgio, T., Donnelly, E., Gao, X., and Clanton, J. (2003). Integrin-mediated targeting of drug delivery to irradiated tumor blood vessels. Cancer Cell *3*, 63–74.

33. Jana, S.S., Bharali, D.J., Mani, P., Maitra, A., Gupta, C.M., and Sarkar, D.P. (2002). Targeted cytosolic delivery of hydrogel nanoparticles into HepG2 cells through engineered Sendai viral envelopes. FEBS Lett. *515*, 184–188.

34. Janes, K.A., Calvo, P., and Alonso, M.J. (2001). Polysaccharide colloidal particles as delivery systems for macromolecules. Adv. Drug Deliv. Rev. *47*, 83–97.

35. Janes, K.A., Fresneau, M.P., Marazuela, A., Fabra, A., and Alonso, M.J. (2001). Chitosan nanoparticles as delivery systems for doxorubicin. J. Control. Release *73*, 255–267.

36. Laakkonen, P., Akerman, M.E., Biliran, H., Yang, M., Ferrer, F., Karpanen, T., Hoffman, R.M., and Ruoslahti, E. (2004). Antitumor activity of a homing peptide that targets tumor lymphatics and tumor cells. Proc. Natl. Acad. Sci. USA *101*, 9381–9386.

37. Laakkonen, P., Porkka, K., Hoffman, J.A., and Ruoslahti, E. (2002). A tumor-homing peptide with a targeting specificity related to lymphatic vessels. Nat. Med. *8*, 751–755.

38. Lanza, G.M., Yu, X., Winter, P.M., Abendschein, D.R., Karukstis, K.K., Scott, M.J., Chinen, L.K., Fuhrhop, R.W., Scherrer, D.E., and Wickline, S.A. (2002). Targeted antiproliferative drug delivery to vascular smooth muscle cells with a magnetic resonance imaging nanoparticle contrast agent: implications for rational therapy of restenosis. Circulation *106*, 2842–2847.

39. Muller, K., Nahde, T., Fahr, A., Muller, R., and Brusselbach, S. (2001). Highly efficient transduction of endothelial cells by targeted artificial virus-like particles. Cancer Gene Ther. *8*, 107–117.

40. Na, K., Lee, E.S., and Bae, Y.H. (2003). Adriamycin loaded pullulan acetate/sulfonamide conjugate nanoparticles responding to tumor pH: pH-dependent cell interaction, internalization and cytotoxicity in vitro. J. Control. Release *87*, 3–13.

41. Na, K., and Bae, Y.H. (2002). Self-assembled hydrogel nanoparticles responsive to tumor extracellular pH from pullulan derivative/sulfonamide conjugate: characterization, aggregation, and adriamycin release in vitro. Pharm. Res. *19*, 681–688.

42. Nahde, T., Muller, K., Fahr, A., Muller, R., and Brusselbach, S. (2001). Combined transductional and transcriptional targeting of melanoma cells by artificial virus-like particles. J. Gene Med. *3*, 353–361.

43. Wickline, S.A., and Lanza, G.M. (2003). Nanotechnology for molecular imaging and targeted therapy. Circulation *107*, 1092–1095.

44. Wickline, S.A., and Lanza, G.M. (2002). Molecular imaging, targeted therapeutics, and nanoscience. J. Cell. Biochem. Suppl. *39*, 90–97.

45. Yoo, H.S., Lee, K.H., Oh, J.E., and Park, T.G. (2000). In vitro and in vivo anti-tumor activities of nanoparticles based on doxorubicin-PLGA conjugates. J. Control. Release *68*, 419–431.

46. Choi, Y., Thomas, T., Kotlyar, A., Islam, M.T., and Baker, J.R., Jr. (2005). Synthesis and functional evaluation of DNA-assembled polyamidoamine dendrimer clusters for cancer cell-specific targeting. Chem. Biol. *12*, 35–43.

47. Dubowchik, G.M., Radia, S., Mastalerz, H., Walker, M.A., Firestone, R.A., Dalton King, H., Hofstead, S.J., Willner, D., Lasch, S.J., and Trail, P.A. (2002). Doxorubicin immunoconjugates containing bivalent, lysosomally-cleavable dipeptide linkages. Bioorg. Med. Chem. Lett. *12*, 1529–1532.

48. Hurwitz, H., Fehrenbacher, L., Novotny, W., Cartwright, T., Hainsworth, J., Heim, W., Berlin, J., Baron, A., Griffing, S., Holmgren, E., et al. (2004). Bevacizumab plus irinotecan, fluorouracil, and leucovorin for metastatic colorectal cancer. N. Engl. J. Med. *350*, 2335–2342.

49. Jendreyko, N., Popkov, M., Beerli, R.R., Chung, J., McGavern, D.B., Rader, C., and Barbas, C.F., 3rd. (2003). Intradiabodies, bispecific, tetravalent antibodies for the simultaneous functional knockout of two cell surface receptors. J. Biol. Chem. *278*, 47812–47819.

50. King, H.D., Dubowchik, G.M., Mastalerz, H., Willner, D., Hofstead, S.J., Firestone, R.A., Lasch, S.J., and Trail, P.A. (2002). Monoclonal antibody conjugates of doxorubicin prepared with branched peptide linkers: inhibition of aggregation by methoxytriethyleneglycol chains. J. Med. Chem. *45*, 4336–4343.

51. King, H.D., Yurgaitis, D., Willner, D., Firestone, R.A., Yang, M.B., Lasch, S.J., Hellstrom, K.E., and Trail, P.A. (1999). Monoclonal antibody conjugates of doxorubicin prepared with branched

linkers: a novel method for increasing the potency of doxorubi-
cin immunoconjugates. Bioconjug. Chem. *10*, 279–288.

52. Trail, P.A., Willner, D., Bianchi, A.B., Henderson, A.J., TrailSmith, M.D., Girit, E., Lasch, S., Hellstrom, I., and Hellstrom, K.E. (1999). Enhanced antitumor activity of paclitaxel in combination with the anticarcinoma immunoconjugate BR96-doxorubicin. Clin. Cancer Res. *5*, 3632–3638.

53. Trail, P.A., Willner, D., Lasch, S.J., Henderson, A.J., Greenfield, R.S., King, D., Zoeckler, M.E., and Braslawsky, G.R. (1992). Antigen-specific activity of carcinoma-reactive BR64-doxorubicin conjugates evaluated in vitro and in human tumor xenograft models. Cancer Res. *52*, 5693–5700.

54. Cortez-Retamozo, V., Backmann, N., Senter, P.D., Wernery, U., De Baetselier, P., Muyldermans, S., and Revets, H. (2004). Efficient cancer therapy with a nanobody-based conjugate. Cancer Res. *64*, 2853–2857.

55. Doronina, S.O., Toki, B.E., Torgov, M.Y., Mendelsohn, B.A., Cerveny, C.G., Chace, D.F., DeBlanc, R.L., Gearing, R.P., Bovee, T.D., Siegall, C.B., et al. (2003). Development of potent monoclonal antibody auristatin conjugates for cancer therapy. Nat. Biotechnol. *21*, 778–784.

56. Francisco, J.A., Cerveny, C.G., Meyer, D.L., Mixan, B.J., Klussman, K., Chace, D.F., Rejniak, S.X., Gordon, K.A., DeBlanc, R., Toki, B.E., et al. (2003). cAC10-vcMMAE, an anti-CD30-monomethyl auristatin E conjugate with potent and selective antitumor activity. Blood *102*, 1458–1465.

57. Hellstrom, I., Hellstrom, K.E., and Senter, P.D. (2001). Development and activities of the BR96-doxorubicin immunoconjugate. Methods Mol. Biol. *166*, 3–16.

58. Willner, D., Trail, P.A., Hofstead, S.J., King, H.D., Lasch, S.J., Braslawsky, G.R., Greenfield, R.S., Kaneko, T., and Firestone, R.A. (1993). (6-Maleimidocaproyl)hydrazone of doxorubicin: a new derivative for the preparation of immunoconjugates of doxorubicin. Bioconjug. Chem. *4*, 521–527.

59. Rader, C., Sinha, S.C., Popkov, M., Lerner, R.A., and Barbas, C.F., 3rd. (2003). Chemically programmed monoclonal antibodies for cancer therapy: adaptor immunotherapy based on a covalent antibody catalyst. Proc. Natl. Acad. Sci. USA *100*, 5396–5400.

60. Trail, P.A., Willner, D., Lasch, S.J., Henderson, A.J., Hofstead, S., Casazza, A.M., Firestone, R.A., Hellstrom, I., and Hellstrom, K.E. (1993). Cure of xenografted human carcinomas by BR96-doxorubicin immunoconjugates. Science *261*, 212–215.

61. Ludwig, D.L., Pereira, D.S., Zhu, Z., Hicklin, D.J., and Bohlen, P. (2003). Monoclonal antibody therapeutics and apoptosis. Oncogene *22*, 9097–9106.

62. Brooks, P.C., Montgomery, A.M., Rosenfeld, M., Reisfeld, R.A., Hu, T., Klier, G., and Cheresh, D.A. (1994). Integrin alpha v beta 3 antagonists promote tumor regression by inducing apoptosis of angiogenic blood vessels. Cell *79*, 1157–1164.

63. Brooks, P.C., Stromblad, S., Klemke, R., Visscher, D., Sarkar, F.H., and Cheresh, D.A. (1995). Antiintegrin alpha v beta 3 blocks human breast cancer growth and angiogenesis in human skin. J. Clin. Invest. *96*, 1815–1822.

64. Rader, C., Popkov, M., Neves, J.A., and Barbas, C.F., 3rd. (2002). Integrin alpha(v)beta3 targeted therapy for Kaposi's sarcoma with an in vitro evolved antibody. FASEB J. *16*, 2000–2002.

65. Brown, K.C. (2004). Hitting the target with bifunctional phage. Chem. Biol. *11*, 1033–1035.

66. Ruoslahti, E. (1996). RGD and other recognition sequences for integrins. Annu. Rev. Cell Dev. Biol. *12*, 697–715.

67. Ruoslahti, E. (2000). Targeting tumor vasculature with homing peptides from phage display. Semin. Cancer Biol. *10*, 435–442.

68. Ruoslahti, E. (2002). Specialization of tumour vasculature. Nat. Rev. Cancer *2*, 83–90.

69. Pasqualini, R., and Ruoslahti, E. (1996). Tissue targeting with phage peptide libraries. Mol. Psychiatry *1*, 423.

70. Pasqualini, R., and Ruoslahti, E. (1996). Organ targeting in vivo using phage display peptide libraries. Nature *380*, 364–366.

71. Arap, W., Haedicke, W., Bernasconi, M., Kain, R., Rajotte, D., Krajewski, S., Ellerby, H.M., Bredesen, D.E., Pasqualini, R., and Ruoslahti, E. (2002). Targeting the prostate for destruction through a vascular address. Proc. Natl. Acad. Sci. USA *99*, 1527–1531.

72. Rajotte, D., and Ruoslahti, E. (1999). Membrane dipeptidase is the receptor for a lung-targeting peptide identified by in vivo phage display. J. Biol. Chem. *274*, 11593–11598.

73. Ruoslahti, E. (2002). Antiangiogenics meet nanotechnology. Cancer Cell *2*, 97–98.

74. Akerman, M.E., Chan, W.C., Laakkonen, P., Bhatia, S.N., and Ruoslahti, E. (2002). Nanocrystal targeting in vivo. Proc. Natl. Acad. Sci. USA *99*, 12617–12621.

75. de Groot, F.M., Broxterman, H.J., Adams, H.P., van Vliet, A., Tesser, G.I., Elderkamp, Y.W., Schraa, A.J., Kok, R.J., Molema, G., Pinedo, H.M., et al. (2002). Design, synthesis, and biological evaluation of a dual tumor-specific motive containing integrin-targeted plasmin-cleavable doxorubicin prodrug. Mol. Cancer Ther. *1*, 901–911.

76. Wermuth, J., Goodman, S.L., Jonczyk, A., and Kessler, H. (1997). Stereoisomerism and biological activity of the selective and superactice $\alpha v\beta 3$ integrin inhibitor cyclo(-RGDfV-) and its retro-inverso peptide. J. Am. Chem. Soc. *119*, 1328–1335.

77. Pasqualini, R., Koivunen, E., and Ruoslahti, E. (1995). A peptide isolated from phage display libraries is a structural and functional mimic of an RGD-binding site on integrins. J. Cell Biol. *130*, 1189–1196.

78. Friedlander, M., Brooks, P.C., Shaffer, R.W., Kincaid, C.M., Varner, J.A., and Cheresh, D.A. (1995). Definition of two angiogenic pathways by distinct alpha v integrins. Science *270*, 1500–1502.

79. Winter, P.M., Caruthers, S.D., Kassner, A., Harris, T.D., Chinen, L.K., Allen, J.S., Lacy, E.K., Zhang, H., Robertson, J.D., Wickline, S.A., et al. (2003). Molecular imaging of angiogenesis in nascent Vx-2 rabbit tumors using a novel alpha(nu)beta3-targeted nanoparticle and 1.5 tesla magnetic resonance imaging. Cancer Res. *63*, 5838–5843.

80. Kim, J.W., and Lee, H.S. (2004). Tumor targeting by doxorubicin-RGD-4C peptide conjugate in an orthotopic mouse hepatoma model. Int. J. Mol. Med. *14*, 529–535.

81. Chen, X., Plasencia, C., Hou, Y., and Neamati, N. (2005). Synthesis and biological evaluation of dimeric RGD peptide-paclitaxel conjugate as a model for integrin-targeted drug delivery. J. Med. Chem. *48*, 1098–1106.

82. Wickham, T.J., Carrion, M.E., and Kovesdi, I. (1995). Targeting of adenovirus penton base to new receptors through replacement of its RGD motif with other receptor-specific peptide motifs. Gene Ther. *2*, 750–756.

83. Dmitriev, I., Krasnykh, V., Miller, C.R., Wang, M., Kashentseva, E., Mikheeva, G., Belousova, N., and Curiel, D.T. (1998). An adenovirus vector with genetically modified fibers demonstrates expanded tropism via utilization of a coxsackievirus and adenovirus receptor-independent cell entry mechanism. J. Virol. *72*, 9706–9713.

84. Chen, L., Zurita, A.J., Ardelt, P.U., Giordano, R.J., Arap, W., and Pasqualini, R. (2004). Design and validation of a bifunctional ligand display system for receptor targeting. Chem. Biol. *11*, 1081–1091.

85. Grifman, M., Trepel, M., Speece, P., Gilbert, L.B., Arap, W., Pasqualini, R., and Weitzman, M.D. (2001). Incorporation of tumor-targeting peptides into recombinant adeno-associated virus capsids. Mol. Ther. *3*, 964–975.

86. Burkhart, D.J., Kalet, B.T., Coleman, M.P., Post, G.C., and Koch, T.H. (2004). Doxorubicin-formaldehyde conjugates targeting alphavbeta3 integrin. Mol. Cancer Ther. *3*, 1593–1604.

87. Su, Z.F., Liu, G., Gupta, S., Zhu, Z., Rusckowski, M., and Hnatowich, D.J. (2002). In vitro and in vivo evaluation of a Technetium-99m-labeled cyclic RGD peptide as a specific marker of alpha(V)beta(3) integrin for tumor imaging. Bioconjug. Chem. *13*, 561–570.

88. Zitzmann, S., Ehemann, V., and Schwab, M. (2002). Arginine-glycine-aspartic acid (RGD)-peptide binds to both tumor and tumor-endothelial cells in vivo. Cancer Res. *62*, 5139–5143.

89. Fahr, A., Muller, K., Nahde, T., Muller, R., and Brusselbach, S. (2002). A new colloidal lipidic system for gene therapy. J. Liposome Res. *12*, 37–44.

90. DeNardo, S.J., Burke, P.A., Leigh, B.R., O'Donnell, R.T., Miers, L.A., Kroger, L.A., Goodman, S.L., Matzku, S., Jonczyk, A., Lamborn, K.R., et al. (2000). Neovascular targeting with cyclic RGD

peptide (cRGDf-ACHA) to enhance delivery of radioimmuno-therapy. Cancer Biother. Radiopharm. *15*, 71–79.

91. Burke, P.A., DeNardo, S.J., Miers, L.A., Lamborn, K.R., Matzku, S., and DeNardo, G.L. (2002). Cilengitide targeting of alpha(v)-beta(3) integrin receptor synergizes with radioimmunotherapy to increase efficacy and apoptosis in breast cancer xenografts. Cancer Res. *62*, 4263–4272.

92. Smith, J.W. (2003). Cilengitide Merck. Curr. Opin. Investig. Drugs *4*, 741–745.

93. Kim, K.K., Kim, R., and Kim, S.H. (1998). Crystal structure of a small heat-shock protein. Nature *394*, 595–599.

94. Kim, C.K., and Lim, S.J. (2002). Recent progress in drug delivery systems for anticancer agents. Arch. Pharm. Res. *25*, 229–239.

95. Assa-Munt, N., Jia, X., Laakkonen, P., and Ruoslahti, E. (2001). Solution structures and integrin binding activities of an RGD peptide with two isomers. Biochemistry *40*, 2373–2378.

96. Gao, A.G., Lindberg, F.P., Dimitry, J.M., Brown, E.J., and Frazier, W.A. (1996). Thrombospondin modulates alpha v beta 3 function through integrin-associated protein. J. Cell Biol. *135*, 533–544.

97. Hellwage, J., Kuhn, S., and Zipfel, P.F. (1997). The human com-plement regulatory factor-H-like protein *1*, which represents a truncated form of factor H, displays cell-attachment activity. Biochem. J. *326*, 321–327.

98. Hermanson, G.T. (1996). Bioconjugate Techniques (San Diego: Academic Press).